Int J Clin Exp Pathol 2017;10(9):10019-10031
www.ijcep.com /ISSN:1936-2625/IJCEP0059551

Original Article

Control-released Alpha-lipoic acid-loaded PLGA microspheres enhance bone formation in type 2 diabetic rat model

Zhan-Zhao Zhang[1*], Lu Song[2*], Zhi-Yong Zhang[1], Ming-Ming Lv[3]

[1]Shanghai Key Laboratory of Tissue Engineering, Department of Plastic and Reconstructive Surgery, Shanghai Ninth People's Hospital, School of Medicine, Shanghai Jiao Tong University, Shanghai, PR China; [2]Department of Neurology, Xin Hua Hospital, School of Medicine, Shanghai Jiao Tong University, Shanghai, PR China; [3]Department of Oral and Maxillofacial-Head and Neck Oncology, Shanghai Ninth People's Hospital, School of Medicine, Shanghai Jiao Tong University, Shanghai 200011, PR China. [*]Equal contributors.

Received June 15, 2017; Accepted August 23, 2017; Epub September 1, 2017; Published September 15, 2017

Abstract: Since diabetes lead to alterations in bone metabolism with reductions in bone mineral content and delayed bone formation, the most effective method for bone regeneration in diabetes remains to be determined. In this study, type 2 diabetes were successfully induced via a high-fat diet and low-dose streptozotocin intraperitoneal injection. Excess reactive oxygen species (ROS) has been implicated in diabetes mellitus. Overexpression of ROS can lead to oxidative stress and subsequently to H_2O_2-mediated impaired proliferation and delayed cellular differentiation. As a result, antioxidant alpha-lipoic acid (ALA)-loaded poly (lactic-co-glycolic acid) (PLGA) microspheres were fabricated using the emulsion solvent evaporation method, and a sustained and controlled release of ALA was observed up to 27 days. It was demonstrated that biodegradable PLGA microspheres loaded with ALA acted as ROS scavengers and partially recover the mesenchymal stem cell proliferation and differentiation. The bone formation of ALA loaded scaffolds in rat cranial bone defects were greater than the prime three-dimensional collagen scaffold. These results suggest the application of ALA loaded PLGA microsphere exhibit good bioactivity and bone forming ability in diabetes.

Keywords: Reactive oxygen species, type 2 diabetes, antioxidant, a-lipoic acid, poly (lactic-co-glycolic acid)

Introduction

With the rapid developments of materials science and biotechnology, application of a three-dimensional (3D) scaffold to the bone defect has been approved as an effective strategy for bone repair and regeneration. However, most of the studies were performed in generally healthy individuals that possessed active tissue regenerative capacity, while their transfer into the clinic in patients with pathological conditions remains controversial [1]. In clinical practice, the clinical failure with delayed union or non-union is much higher in those suffering from pathological conditions that limit the capacity of neovascularization and osteogenesis, e.g. diabetes, osteoporosis or hypertonia [2, 3]. Thus, it is critical to address the need of bone regeneration in such pathological conditions.

Type 2 Diabetes mellitus (DM), a metabolic disease that is primarily characterized by abnormal regulation of glucose metabolism, afflicts over 190 million people worldwide [4, 5]. DM has been associated with various musculoskeletal abnormalities that alter the normal bone healing program, such as increased risk of bone fractures, delayed fracture healing, and osteoporosis, etc. [6]. Previous studies on the effect of experimental diabetes on the bone healing have demonstrated that there is an evidence for decreased progenitor cell proliferation [7, 8], reduced cartilage formation and premature cartilage resorption [5], delayed cellular differentiation and biomechanically inferior repair [9, 10].

In the recent studies, substantial and growing evidences have proven that the hyperglycemia

associated with diabetes could dramatically increase the level of reactive oxygen species (ROS) in various cell types [11], and the impaired oxidant/antioxidant balance might be one of the critical biological mechanisms underlying poor bone formation in uncontrolled diabetes. ROS is an important inflammatory mediator with local and distant patho-physiological effects under pathological conditions [12], and its overproduction is known to be able to subsequently suppress the migration, proliferation, and osteogenesis capacity of progenitor cells during the healing period [5]. Alternatively, scavenging ROS with antioxidant remarkably rescues the decreased cell viability and dysfunction [3].

Alpha-lipoic acid (ALA), an essential free radical scavenger that play a crucial role in the mitochondrial respiratory pathway [13], has attracted considerable attention and is used in the treatment of several inflammatory related diseases [14-16]. However, the good solubility of ALA leads to the immediate release spike in plasma within 1 h after oral administration which is fast eliminated subsequently [17]. Local drug delivery system made of biodegradable materials, such as microspheres and scaffolds, is an effective method to improve drug bioavailability [18]. They allow for precise control over local drug release to increase bioavailability and protect encapsulated components against degradation to prolong drug activity.

As a result, the aim of our study was to assess if local introduction of ALA to the collagen scaffold could facilitate the scaffold with better osteogenesis in diabetes mellitus animal model. In this work, the collagen scaffold was functionalized with ALA-loaded poly (lactic-co-glycolic acid) (PLGA) microspheres, in order to deliver a controlled and prolonged release of ALA.

Materials and methods

Materials

Collagen was obtained from Sichuan Mingrang Tech., China. ALA, PLGA, N-(3-(dimethylamino) propyl)-N-ethylcarbodiimide hydrochloride crystalline (EDC) and N-hydroxysuccinimide (NHS) were purchased from Sigma Aldrich. A Cell Counting Kit-8 (CCK-8) was obtained from Dojindo. Polyvinyl Alcohol (PVA) and dichloromethane were purchased from Aladdin, China.

Scaffolds fabrication and surface characterization

ALA-loaded PLGA microspheres were fabricated using the single emulsion solvent evaporation method [19]. Briefly, PLGA was dissolved in dichloromethane with ALA (the final concentration is 2% W/V) and sonicated for 15 min to obtain a homogeneous dispersion. Then the mixture was then slowly dropped into 3% (w/v) aqueous PVA solution. After that, the mixture was magnetic-stirred to volatilize the solvent for 6 h at room temperature, and then collected by centrifugation (500 g, 5 min). The obtained microspheres were washed three times with distilled water and lyophilized in a freeze-dryer for 48 h.

Collagen scaffolds (COL) were prepared as previously described. Briefly, 1% collagen solution (1% W/V in ddH_2O) was obtained under magnetic stirring. Then, 0.1 M EDC and 0.025 M NHS were added under stirring, and the mixture was held for 1 h at RT to form a hydrogel by self-crosslinking. The hydrogels were frozen overnight at -80°C and subsequently lyophilized at -50°C [20]. To incorporate the PLGA microspheres into the scaffolds (PLGA/COL), 7 mg of PLGA microspheres was mixed well with 10 ml of collagen slurry (the final concentration of PLGA is 0.07%). The surface and pore morphologies and pore size distributions of the scaffolds were observed using scanning electron microscopy (Hitachi, Ibaraki, Japan) at an accelerating voltage of 10 kV.

Release properties

To determine the ALA release kinetic from the PLGA microspheres, 1 mg of PLGA microspheres were added to 5 ml of PBS in a 10 ml tube and then shaken at 37°C. At certain time points, the supernatant was removed and an equal volume of fresh PBS was added. The concentration of ALA in the supernatant was determined using a UV spectrophotometer as above.

Isolation and Identification of bone marrow derived mesenchymal stem cells

Rat bone marrow derived mesenchymal stem cells (BMSCs) were obtained as previously

Table 1. Summary of primer sequences

Sequences of primers for PCR		
Gene name	Forward or Reverse	Sequence (5'-3')
BMP2	Forward	CGTCAAGCCAAACACAAACA
	Reverse	AGTCATTCCACCCCACATCA
COL1	Forward	CGTGGAAACCTGATGTATGCT
	Reverse	ACTCCTATGACTTCTGCGTCTG
ALP	Forward	GAAAGAGAAAGACCCCAGTTAC
	Reverse	ATACCATCTCCCAGGAACAT
Runx2	Forward	CGAAATGCCTCTGCTGTTAT
	Reverse	CGTTATGGTCAAAGTGAAACTCT
β-actin	Forward	CCTCTATGCCAACACAGT
	Reverse	AGCCACCAATCCACACAG

described [21]. Cells were cultured in Dulbecco's modified Eagle's media (DMEM) containing 10% fetal bovine serum (FBS) and 1% penicillin-streptomycin. Passage 2-3 BMSCs were used for the experiments. To evaluate surface markers, antibodies against CD29, CD31, CD44, CD45 and CD90 were used. Cell fluorescence was determined using a FACS flow cytometer (BD Biosciences, San Jose, CA, USA).

Analysis of cell proliferation

The microspheres were sterilized with ethylene oxide prior to use. Indirect culture method was used to observe the effect of the ALA release. 1 × 10^4 cells were seeded onto each well of 24 well-plates and were randomized to incubate with one of the following factors: 1) normal serum (NS), 2) diabetic serum (DS) and 3) DS + ALA/PLGA. The ALA/PLGA were placed on the top of the cells separated by a culture insert (0.32 cm^2, pore diameter 0.4 um, Millipore). The normal and diabetic serum were acquired from normal and diabetic rats, respectively. For the proliferation, the cell proliferation was assessed using a CCK-8 according to the manufacturer's instruction at each time point (1, 3, 5 and 7 days). The absorbance was measured at 450 nm using a microplate reader (Thermo Electron Corporation, Waltham, MA, USA). Intracellular ROS measurement ROS was measured using a non-fluorescent probe, 2,7-diacetyl dichlorofluorescein (DCFH-DH) that can penetrate into the intracellular matrix of cells, where it is oxidized by ROS to fluorescent dichlorofluorescein (DCF) [14]. Briefly, an aliquot of isolated cells (8 × 10^6 cells/ml) were made up to a final volume of 2 ml in normal phosphate buffered saline (pH 7.4). 1 ml aliquot of cells was taken to which 1 μl DCFH-DA (1 mg/mL) was added and incubated at 37°C for 30 min under dark condition. Fluorescent measurements were made with excitation and emission at 485 ± 10 and 530 ± 12.5 nm, respectively using a multimode reader (Teccan, Austria). Images were taken on an epifluorescent microscope (Nikon, Eclipse TS100, Japan) with a digital camera (Nikon 4500 Coolpix, Japan).

Intracellular ROS measurement

2,7-diacetyl dichlorofluorescein (DCFH-DH) was used to measure the intracellular ROS [22]. Briefly, 1 ml aliquot of isolated cells (8 × 10^6 cells/ml) were made in PBS, then 1 μl DCFH-DA (1 mg/mL) was added and incubated at 37°C for 30 min under dark condition. Images were taken on a fluorescent microscope (FV1000, Olympus, Japan).

Alkaline phosphatase (ALP) and alizarin red staining

At day 7 after osteogenic induction, the cells were fixed for ALP staining and subsequent imaging evaluation using HP Scanjet G3110 Photo Scanner. ALP activity after 7 and 14 days of culture was quantified using the QuantiChrom TM Alkaline Phosphatase Assay Kit (BioAssay Systems, CA, USA), and the total protein content was assessed with the BCA Protein Assay Kit (Thermo Scientific). At day 14 after osteogenic induction, cells were fixed in 4% paraformaldehyde for 15 min and were then incubated with 40 mM alizarin red (AR) staining solution for 15 min at room temperature. For quantification of the mineralization, the mineralized matrix nodules were dissolved in 10% (w/v) cetylpyridinium chloride (Aladdin), and the absorbance was measured at 450 nm using a microplate reader.

Quantitative real-time polymerase chain reaction (RT-qPCR)

The expressions of genes associated with osteogenesis were assessed by RT-qPCR. For this, BMSCs were seeded at 1 × 10^4 onto each well of 24-well plates. After 6 h, 1 ml osteogenic induction media consisting of DMEM supplemented with 10% FBS, 50 mg/ml of ascorbic

acid, 10 mM β-glycerophosphate, and 10 nM dexamethasone was added, and the transwell insert containing microspheres was placed onto each well. After 7 and 14 days of the indirect culture, the total RNA was prepared using TRIzol reagent (Invitrogen) to determine the osteogenesis related gene expression [Alkaline phosphatase (ALP), Collagen type 1 (COL1), Bone morphogenetic protein-2 (BMP2) and Runt-related transcription factor 2 (RUNX2)] and real-time PCR was conducted using SYBR GreenER qPCR SuperMix reagents (Invitrogen). The relative expression was obtained by normalizing the mean cycle threshold (Ct) value of each target gene with the Ct value of the house keeping gene (β-actin). The primer sequences of the genes are summarized in **Table 1**.

Viability of BMSCs in collagen substrates

Fluorescent microscopy was used to study the viability of BMSCs culture on 3D collagen scaffolds. The scaffolds were cultured with BMSCs in 24-well culture plates. At 48 h after cell seeding, the scaffolds were washed with PBS for 5 min and stained using a live/dead cell imaging kit (Invitrogen, CA, USA) according to manufacturer's instructions. After that, the stained cells were examined with an inverted fluorescence microscope (Carl Zeiss Meditec, Jena, Germany).

Rat type 2 diabetes model

A high-fat diet and low-dose streptozotocin (STZ) intraperitoneal injection was administered to 40 rats to induce type 2 diabetes as previously reported [5, 23]. The treatment study protocol was approved by the Ethical Committee of Shanghai Ninth People's Hospital Affiliated Shanghai Jiao Tong University School of Medicine, and the National Institutes of Health Guide concerning the Care and Use of Laboratory Animals. After consuming a high-fat diet with a total calorific value 44.3 kJ/kg for 4 weeks, rats in the DM group were intraperitoneally injected with 30 mg/kg of STZ. A same volume of vehicle buffer was injected in the control group. Four weeks following the STZ injections, rats with blood glucose levels of ≥16.7 mmol/L were considered diabetic and were allowed to continue to feed on a high-fat diet until the end of the study. The diabetic rats were then randomly divided into a COL group (collagen scaffold, n = 6), and a ALA/PLGA/COL group (Collagen scaffolds with ALA-loaded PLGA microspheres, n = 6). The collagen scaffolds implanted in the normal rats were served as the control (n = 6).

Critical-sized cranial bone defect and transplantation

A rat critical-sized cranial bone defect model was performed as previously described [21]. Briefly, the rats were anesthetized by pentobarbital intraperitoneal injection (Nembutal 3.5 mg/100 g). Then, a 2.0 cm sagittal incision was made in the middle of the scalp to expose the calvarium. The defect was created by means of a 5-mm diameter trephine (Nouvag AG, Goldach, Switzerland). After the scaffold was implanted, the incision was closed. 8 weeks after surgery, rats were sacrificed for Micro-CT measurement and histological analysis.

Micro-CT measurement

The defect sites were dissected, soaked in 4% paraformaldehyde, and scanned at a resolution of 10 μm using a Micro-CT (GE Healthcare, Milwaukee, USA). After scanning, 3D images of the samples were reconstructed based on the slices and bone volume per tissue volume (BV/TV) of the defect sites in all groups was statistically analyzed using the CTAn software (Bruker Corporation, Kontich, Belgium).

Histological analysis

After being examined by micro-CT, the samples were decalcified in 10% EDTA for 21 days. After complete decalcification, the samples were dehydrated in increasing grades of ethanol and embedded in paraffin wax. Then, the paraffin-embedded samples were sectioned into 5 μm thick sections using a microtome and stained with hematoxylin and eosin. To observe type I collagen, Masson's trichrome staining was performed. The results of staining were observed using a light microscope.

Statistical analysis

Numerical data were presented as mean ± standard deviation and analysis of variance (ANOVA) and post-hoc Holm-Sidak multiple comparison tests was performed to determine the statistical significance between experimental groups with GraphPad Prism 6 (San Diego,

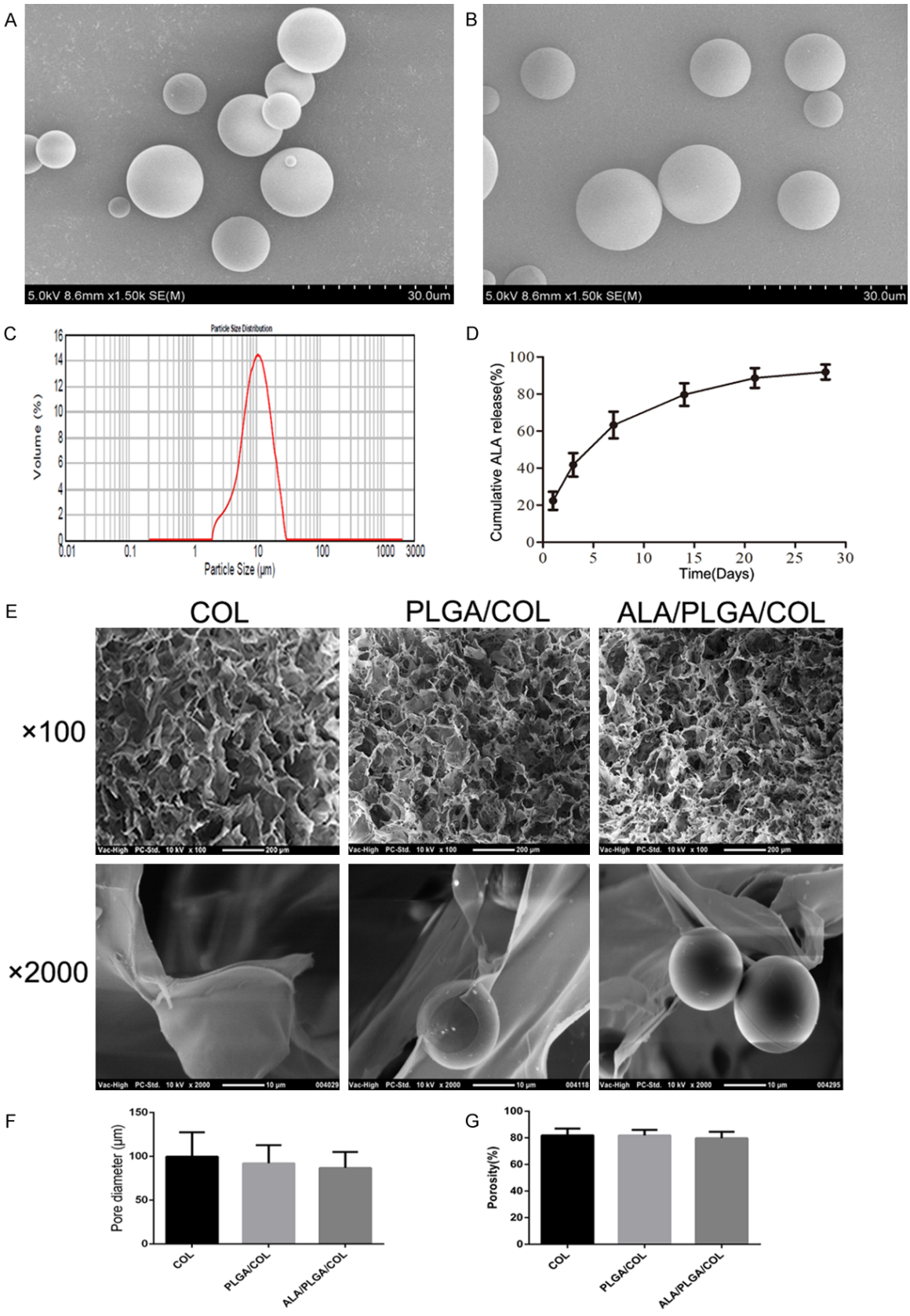

Figure 1. Scanning electron microscope (SEM) images of (A) blank PLGA microspheres and (B) ALA-loaded PLGA microspheres. Magnification, × 1500. (C) The average particle sizes of ALA-loaded PLGA microspheres. (D) Cumulative in vitro release profile of ALA from PLGA microspheres. (E) 100 × and 2000 × magnification of SEM images of COL, PLGA/COL and ALA/PLGA/COL scaffolds. The pore diameter (F) and porosity (G) of the scaffolds.

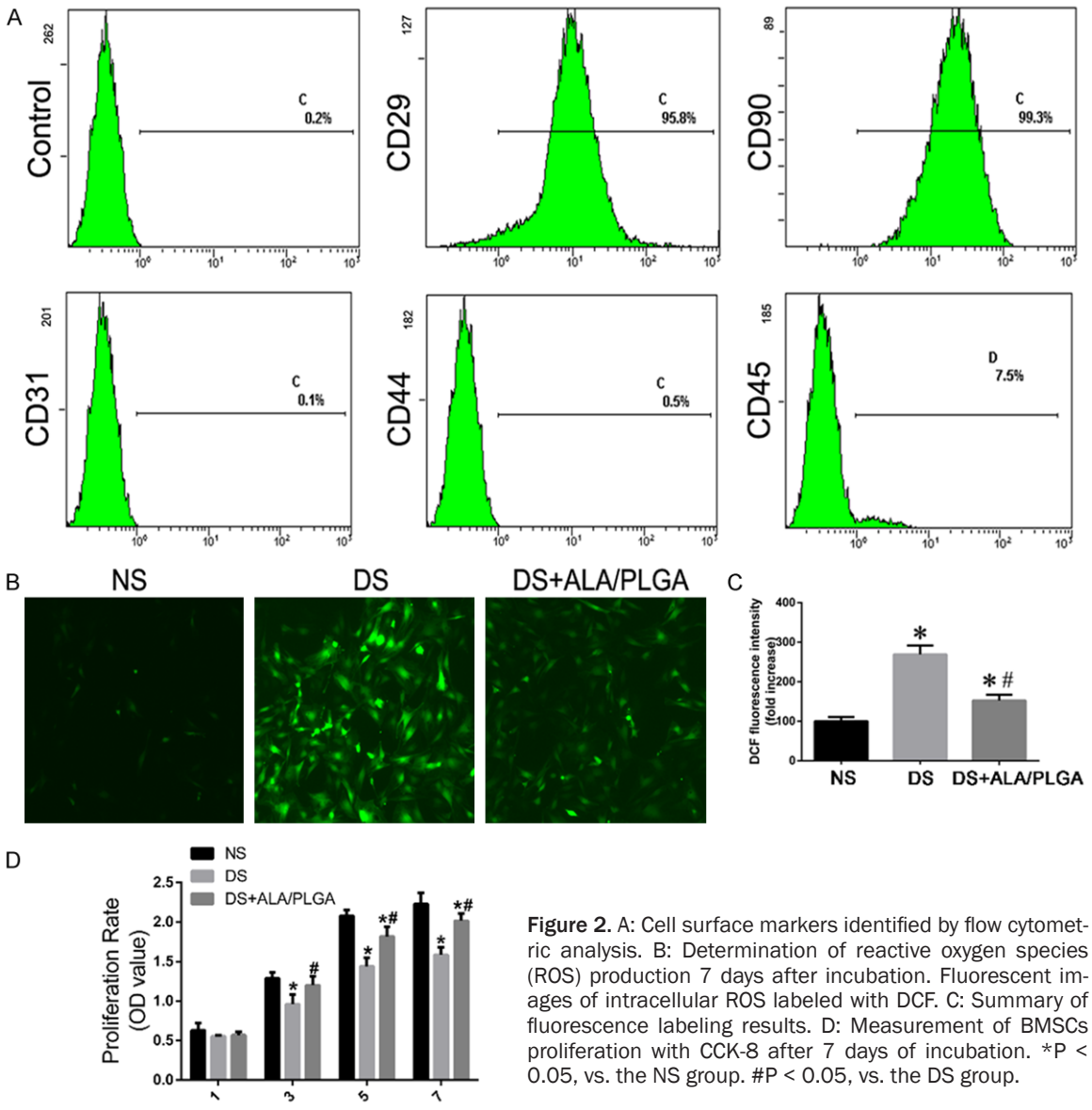

Figure 2. A: Cell surface markers identified by flow cytometric analysis. B: Determination of reactive oxygen species (ROS) production 7 days after incubation. Fluorescent images of intracellular ROS labeled with DCF. C: Summary of fluorescence labeling results. D: Measurement of BMSCs proliferation with CCK-8 after 7 days of incubation. *P < 0.05, vs. the NS group. #P < 0.05, vs. the DS group.

CA, USA). A value of $P < 0.05$ was regarded as statistically significant difference.

Results

Characterization of PLGA microspheres

As shown in scanning electron microscopy (SEM) images, the blank PLGA microspheres showed smooth surface and spherical shape (**Figure 1A**). There was no significant difference in morphology between the blank PLGA microspheres and ALA-loaded PLGA microspheres (**Figure 1B**). The particle size distribution (**Figure 1C**) was in the range of 2~20 μm (average particle size 11.26 μm). The *in vitro* release profile of the ALA from the microspheres was analyzed by UV spectrophotometry (**Figure 1D**). Approximately 42% of the initially incorporated ALA was released from the microspheres in the first three days. After the initial burst release, the ALA was released in a sustained manner over 27 days. At the end-point of the release study, ALA-loaded microspheres had released 92% of the initially incorporated content.

Characterization of scaffolds

The COL scaffolds exhibited an interconnected porous network (**Figure 1E**), and the PLGA

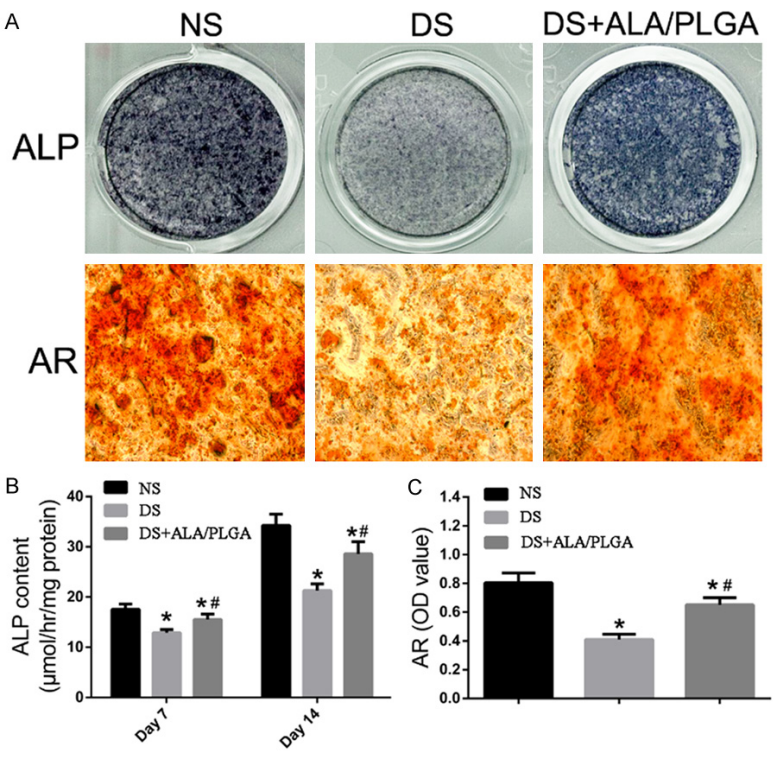

Figure 3. The effect on osteogenic differentiation of BMSCs. A: Representative images of ALP and Alizarin red (AR) staining. B: ALP activity results. C: Summary of AR staining results. *P < 0.05, vs. the NS group. #P < 0.05, vs. the DS group.

microspheres were uniformly distributed within the collagen matrix. The mean pore size and porosity of COL scaffolds were 99.8 μm and 81.9%, respectively. The incorporation of ALA loaded PLGA microspheres into the scaffolds slightly reduced the pore size and the porosity (**Figure 1F**, **1G**).

Characterization of BMSCs

As shown in **Figure 2A**, the cell surface markers identified by flow cytometric assay revealed they were positive for the MSC surface markers CD29 and CD90, but negative for the hematopoietic and endothelial surface markers CD31, CD44 and CD45.

Intracellular ROS measurement

The intracellular ROS production in cultured BMSCs was determined with the analyzing intensity of DCF fluorescence 7 days after culture, and the results (**Figure 2B**, **2C**) showed markedly higher intensity in DS group than that in the NS group, while the incubation of BMSCs with DS supplemented with ALA/PLGA significantly attenuated ROS generation.

Cell proliferation and viability

We further investigated the role of antioxidant ALA in diabetic serum-induced suppressed BMSC function and decreased proliferation. A CCK-8 assay was used to evaluate the effect of the diabetic serum and ALA/PLGA on cell proliferation. As showed in **Figure 2D**, the cell number gradually increased as the culture time prolonged in all groups. There were no significant differences between the NS and DS group at day 1. The cell viability was statistically lower in DS group, even more obvious after 7 days of incubation. The suppression of ROS by ALA obviously improve proliferation of BMSCs cultured with DS.

Osteogenic activity of BMSCs

ALP and AR staining were used to evaluate the osteogenic activity of BMSCs cultured with different culture mediums, and both groups revealed osteogenic differentiation when subjected to osteogenic supplements. However, in the BMSCs stimulated by DS, the ALP activity and mineralized nodules were more distinct in ALA/PLGA group (**Figure 3A**). The ALP activity of BMSCs cultured in different groups was quantitatively evaluated at 7 and 14 days respectively (**Figure 3B**). With culture time increasing from 7 to 14 days, an increase in ALP activity was observed in all the three groups. However, the ALP activity of BMSCs in the DS group was significantly lower than that in the normal control groups at 7 and 14 days. The impaired osteogenic differentiation was partially recovered by ALA/PLGA. Similar result was revealed by the quantitative results of AR staining (**Figure 3C**).

Osteogenic gene expression

The mRNA expression levels of ALP, RUNX2, BMP2 and COL1 in BMSCs cultured in different

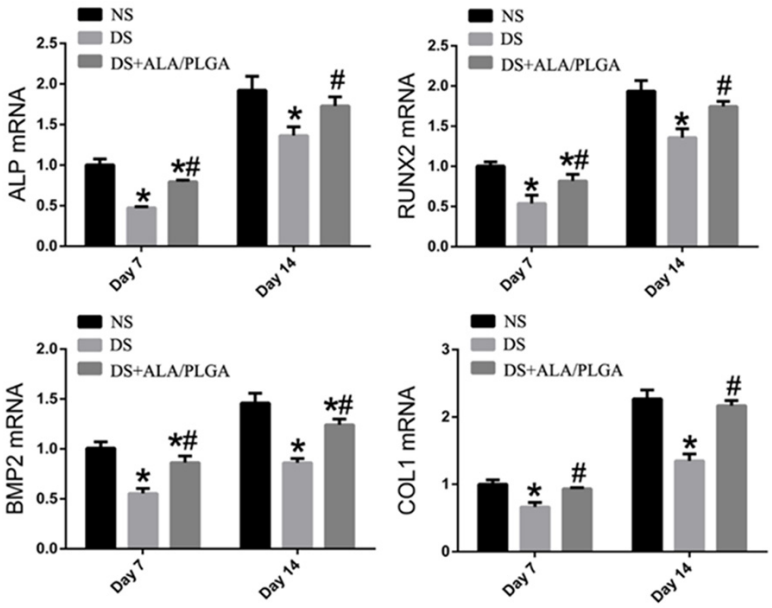

Figure 4. RT-qPCR results of osteogenesis marker genes (ALP, RUNX2, BMP2, COL1) after 7 and 14 days of incubation. The results are represented as relative ratio to the NS group. *P < 0.05, vs. the NS group. #P < 0.05, vs. the DS group.

groups were examined by quantitative real-time RT-PCR and are shown in **Figure 4**. On day 7, the expression levels of osteogenic genes were significant lower in the DS group. However, after PLGA/ALA was added, both the expression levels were significantly higher than those in the DS groups.

Biocompatibility of the scaffolds

Prior to the in vivo study, the biocompatibility of the scaffolds was confirmed by incubation with BMSCs. As shown in **Figure 5A**, live-dead cell staining revealed a lot of viable cells (green) and a few apoptotic cells (red) could be found on the prime scaffolds in the NS group after 3 days of incubation. The results indicated that all scaffolds can support the adhesion and proliferation of BDSCs without eliciting side effects. Incubation of BMSCs with DS significantly impaired the cell viability, while the suppression of ROS by ALA improve the cell attachment and viability (**Figure 5B**).

Construction of the type 2 diabetes model

The plasma glucose levels and insulin tolerance test of the STL and vehicle injection groups were measured every week. A diabetic model analogous to type 2 diabetes mellitus was identified with hyperglycemia and insulin resistance (**Figure 6**). 4 weeks after STZ injection, the glucose levels in the DM indicated hyperglycemia when compared to the control groups at 120 min after glucose injection. Insulin tolerance test indicated that following insulin administration, the glucose concentrations declined slowly or stayed constant in the DM for 30 min following the glucose injection when compared to the control. Five rats were excluded from the experiment (2 rats did not achieve hyperglycemia, and 3 rats were induced type 1 diabetes mellitus with plasma glucose levels up to 26 mmol/L).

Micro-CT measurement

Micro-CT was used to evaluate the newly regenerated bone at 8 weeks post operation. Micro CT images clearly depicted the osteogenesis in both control and diabetic group, while the control group showed generally more bone formation. Almost minor regenerated bone tissue was found in the diabetic group, while the scaffolds loaded with ALA-PLGA significantly increased new bone formation compared with diabetic group. (**Figure 7A**) Quantitative analysis showed that both bone volume around the 3D collagen scaffolds was in the order: control > diabetes + ALA/PLGA > diabetes (**Figure 7B**).

Histological examination

The histological images showed similar results; the ALA/PLGA loaded scaffold significantly promote new bone formation compared with diabetic group. In the control group, bone defects were almost completely filled with bone, which confirmed the good bioactivity and biodegradability of three-dimensional collagen scaffolds. However, the quantity and quality of bone formation was greatly impaired under diabetic condition, very little newly regenerated bone predominantly present at the defect edges and the majority of the defect space was occupied with fibrous connective tissues. A large amount

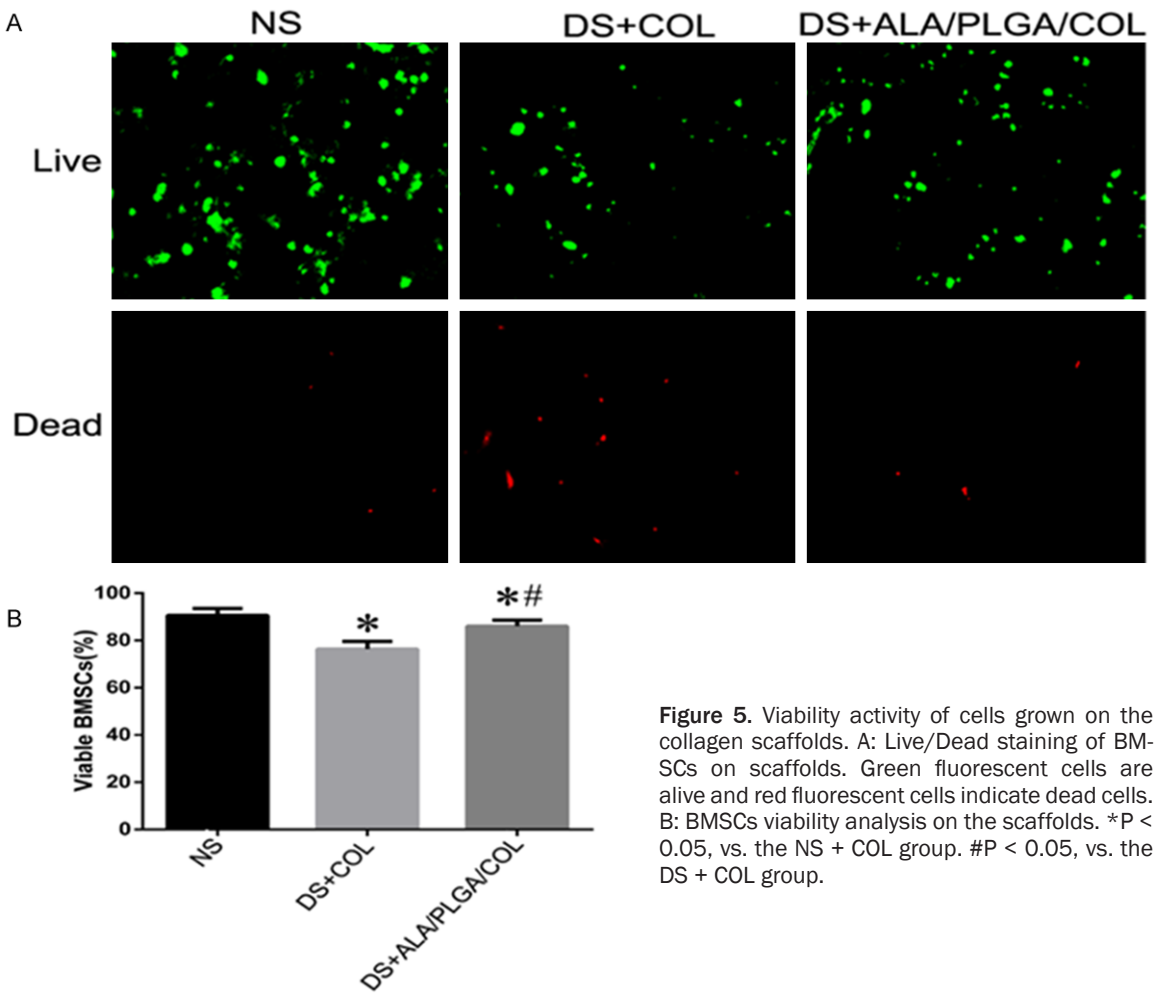

Figure 5. Viability activity of cells grown on the collagen scaffolds. A: Live/Dead staining of BMSCs on scaffolds. Green fluorescent cells are alive and red fluorescent cells indicate dead cells. B: BMSCs viability analysis on the scaffolds. *P < 0.05, vs. the NS + COL group. #P < 0.05, vs. the DS + COL group.

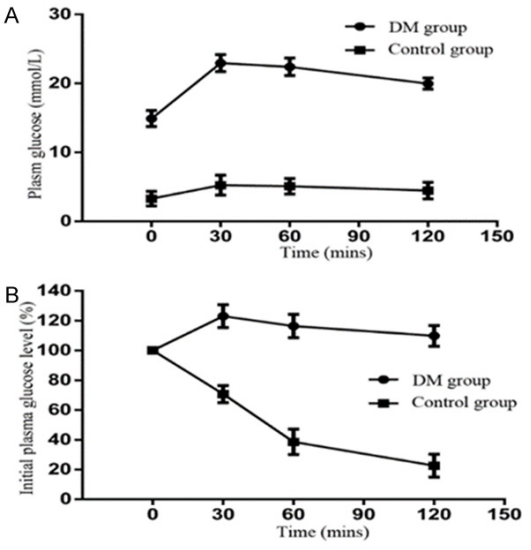

Figure 6. A: Plasma glucose during intraperitoneal glucose tolerance test in rats after 4 weeks STZ injection (DM group) or vehicle injection (control group). B: Percentage of initial glucose level during insulin tolerance test in DM and control group 4 weeks after injection.

of newly formed bone was observed in the defect treated with ALA/PLGA loaded scaffold (**Figure 7C**).

Discussion

Early events associated with bone healing in patients with type 2 diabetes mellitus appear to be delayed, while the underlying biological mechanisms are not yet well understood. ROS is an important inflammatory mediator with local and distant patho-physiological effects under pathological conditions [3, 24]. In this study, ALA-PLGA microsphere was chosen to examine the role of controlled released of antioxidant in osteogenesis for tissue engineering in type 2 diabetic rat model, and we demonstrated the feasibility of repairing critical-sized cranial bone defects with ALA-PLGA microspheres loaded 3D scaffolds made of collagen in rats with uncontrolled diabetes mellitus.

To a great extent, we had shown that diabetic condition induced the overproduction of ROS,

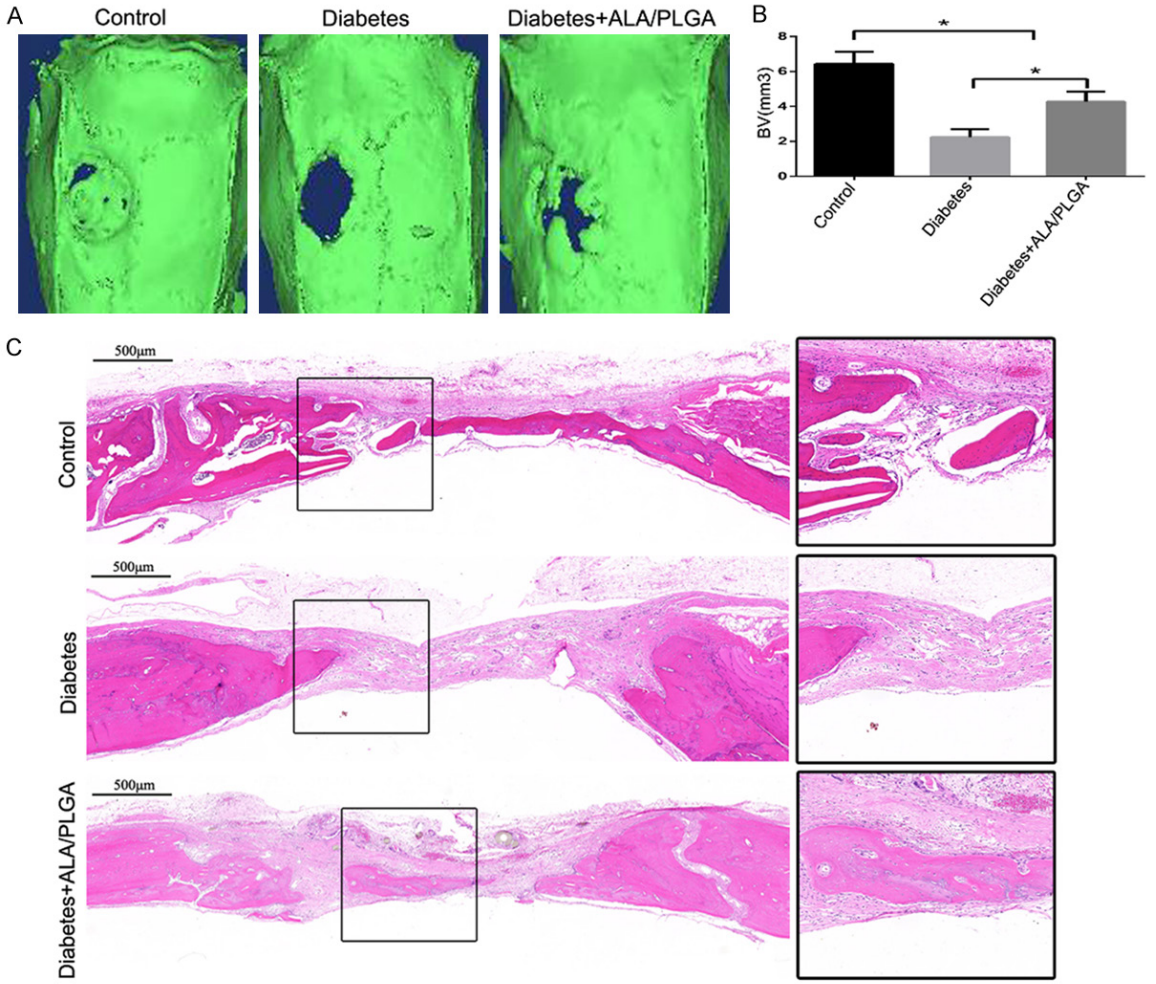

Figure 7. Bone regeneration of calvarial defect implanted with collagen scaffolds. A: Micro-CT scan of calvarial bone defect at 3 months after surgery. B: Bone volume. *P < 0.05. C: H&E stained tissue sections of bone regeneration in the defect area of healthy (Control) and diabetic (Diabetes) rats implanted with collagen scaffolds and diabetic rats implanted with ALA/PLGA loaded collagen scaffolds (Diabetes + ALA/PLGA) at 3 months after surgery.

resulting in reduced cellular proliferation and impaired cellular function of BMSCs in vitro and compromised bone formation within the 3D collagen scaffolds in vivo. Furthermore, we also demonstrated that the scavenging ROS with ALA-PLGA could significantly attenuated ROS induced BMSCs dysfunction, with marked increase in proliferation and osteogenesis ability, such as ALP activity and BMP2, RUNX2 and COL1 expression. In vivo study also revealed an improved osteogenesis of ALA-PLGA loaded collagen scaffolds in diabetes.

Hyperglycemia and the associated increase in oxidative stress, which subsequently disrupts the cellular oxidant/antioxidant balance, are cited as potential factors leading to a change in cellular behavior [25, 26]. Hyperglycemia-induced ROS have been proposed to be generated via several mechanisms including glucose autoxidation, protein glycation, advanced glycation end product formation, increased polyol pathway activity and overproduction by mitochondria [27-29]. ROS activated by hyperglycemia could damage BMSCs proteins, lipids, nucleic acids and other macromolecular substances that have physiological functions [17, 30], resulting in low metabolic activity and cell cycle arrest by activating apoptosis [3]. It can affect the differentiation of BMSCs and even cause cell death to reduce the effectiveness of defect repair [31]. In this study, overexpression

of ROS was revealed in DS group with impaired BMSC proliferation and differentiation.

Since the over-oxidation and generation of free radicals are two common factors that result in the occurrence of inflammation and impaired tissue repair, antioxidant has attracted considerable attention. In the present study, the 3D collagen scaffold was functionalized with ALA-loaded PLGA microspheres, in order to deliver a localized controlled release of ALA as a primary defense against free radicals. PLGA microsphere was chosen as the drug carrier because of its excellent biocompatibility, non-toxic and controlled degradable rate [32-34]. In the present study, the obtained ALA-loaded PLGA microspheres were uniform and spherical with a size range from 2 μm to 18 μm, with a slowly sustained release of ALA for over 27 days. As expected, scavenging ROS with antioxidant remarkably rescue the decreased cell viability and dysfunction were confirmed with indirect culture method using a culture insert. In vivo study also revealed the superior osteogenesis potential of the controlled released of ALA via a rat critical-size calvarial defect model.

Besides, the pore size and porosity are important indexes during the design of bone tissue engineering scaffolds, and a desirable scaffold should provide an appropriate pore space to facilitate cell infiltration and tissue formation [35-37]. In our study, 3D collagen scaffolds were chosen as a model biomaterial and the pore size of the collagen scaffold was about 100 μm with a porosity value about 80%, which is suitable for osteoblast migration, vascular ingrowth and nutrition supply. This was also confirmed by the rat critical-size calvarial defect model implanted with prime collagen scaffolds.

Conclusion

This study demonstrated that the ALA-PLGA loaded 3D collagen possesses promising capacity in healing critical-sized bone defect in diabetic animals, although its therapeutic efficacy could be considerably compromised by the pathological condition. The impaired oxidant/antioxidant balance might be one of the critical biological mechanisms underlying poor bone formation in uncontrolled diabetes, and local delivery of antioxidant provides an effective and attractive strategy for bone defect treatment under diabetic condition.

Disclosure of conflict of interest

None.

Address correspondence to: Zhi-Yong Zhang, Shanghai Key Laboratory of Tissue Engineering, Department of Plastic and Reconstructive Surgery, Shanghai Ninth People's Hospital, School of Medicine, Shanghai Jiao Tong University, Shanghai 200011, PR China. E-mail: drzhiyong@126.com; Ming-Ming Lv, Department of Oral and Maxillofacial-Head and Neck Oncology, Shanghai Ninth People's Hospital, School of Medicine, Shanghai Jiao Tong University, Shanghai 200011, PR China. E-mail: lvmingming001@163.com

References

[1] Wang ZX, Chen C, Zhou Q, Wang XS, Zhou G, Liu W, Zhang ZY, Cao Y and Zhang WJ. The treatment efficacy of bone tissue engineering strategy for repairing segmental bone defects under osteoporotic conditions. Tissue Eng Part A 2015; 21: 2346-2355.

[2] Schumann P, Lindhorst D, Kampmann A, Gellrich NC, Krone-Wolf S, Meyer-Lindenberg A, von See C, Gander T, Lanzer M, Rucker M and Essig H. Decelerated vascularization in tissue-engineered constructs in association with diabetes mellitus in vivo. J Diabetes Complications 2015; 29: 855-864.

[3] Feng YF, Wang L, Zhang Y, Li X, Ma ZS, Zou JW, Lei W and Zhang ZY. Effect of reactive oxygen species overproduction on osteogenesis of porous titanium implant in the present of diabetes mellitus. Biomaterials 2013; 34: 2234-2243.

[4] Colombo JS, Balani D, Sloan AJ, Crean SJ, Okazaki J and Waddington RJ. Delayed osteoblast differentiation and altered inflammatory response around implants placed in incisor sockets of type 2 diabetic rats. Clin Oral Implants Res 2011; 22: 578-586.

[5] Yu M, Zhou W, Song Y, Yu F, Li D, Na S, Zou G, Zhai M and Xie C. Development of mesenchymal stem cell-implant complexes by cultured cells sheet enhances osseointegration in type 2 diabetic rat model. Bone 2011; 49: 387-394.

[6] Brown ML, Yukata K, Farnsworth CW, Chen DG, Awad H, Hilton MJ, O'Keefe RJ, Xing L, Mooney RA and Zuscik MJ. Delayed fracture healing and increased callus adiposity in a C57BL/6J murine model of obesity-associated type 2 diabetes mellitus. PLoS One 2014; 9: e99656.

[7] Ogasawara A, Nakajima A, Nakajima F, Goto K and Yamazaki M. Molecular basis for affected cartilage formation and bone union in fracture healing of the streptozotocin-induced diabetic rat. Bone 2008; 43: 832-839.
[8] Gandhi A, Beam HA, O'Connor JP, Parsons JR and Lin SS. The effects of local insulin delivery on diabetic fracture healing. Bone 2005; 37: 482-490.
[9] Follak N, Kloting I and Merk H. Influence of diabetic metabolic state on fracture healing in spontaneously diabetic rats. Diabetes Metab Res Rev 2005; 21: 288-296.
[10] Follak N, Kloting L, Wolf E and Merk H. Delayed remodeling in the early period of fracture healing in spontaneously diabetic BB/OK rats depending on the diabetic metabolic state. Histol Histopathol 2004; 19: 473-486.
[11] Waddington RJ, Alraies A, Colombo JS, Sloan AJ, Okazaki J and Moseley R. Characterization of oxidative stress status during diabetic bone healing. Cells Tissues Organs 2011; 194: 307-312.
[12] Di Meo S, Reed TT, Venditti P and Victor VM. Role of ROS and RNS sources in physiological and pathological conditions. Oxid Med Cell Longev 2016; 2016: 1245049.
[13] Uyar IS, Onal S, Akpinar MB, Gonen I, Sahin V, Uguz AC and Burma O. Alpha lipoic acid attenuates inflammatory response during extracorporeal circulation. Cardiovasc J Afr 2013; 24: 322-326.
[14] Zhang WJ and Frei B. Alpha-lipoic acid inhibits TNF-alpha-induced NF-kappaB activation and adhesion molecule expression in human aortic endothelial cells. FASEB J 2001; 15: 2423-2432.
[15] Kagan VE, Shvedova A, Serbinova E, Khan S, Swanson C, Powell R and Packer L. Dihydrolipoic acid--a universal antioxidant both in the membrane and in the aqueous phase. Reduction of peroxyl, ascorbyl and chromanoxyl radicals. Biochem Pharmacol 1992; 44: 1637-1649.
[16] Marfella R, Barbieri M, Sardu C, Rizzo MR, Siniscalchi M, Paolisso P, Ambrosino M, Fava I, Materazzi C, Cinquegrana G, Gottilla R, Elia LR, D'Andrea D, Coppola A, Rambaldi PF, Mauro C, Mansi L and Paolisso G. Effects of alpha-lipoic acid therapy on sympathetic heart innervation in patients with previous experience of transient takotsubo cardiomyopathy. J Cardiol 2016; 67: 153-161.
[17] Bai MY and Hu YM. Development of alpha-lipoic acid encapsulated chitosan monodispersed particles using an electrospray system: synthesis, characterisations and anti-inflammatory evaluations. J Microencapsul 2014; 31: 373-381.
[18] Li H, Liao H, Bao C, Xiao Y and Wang Q. Preparation and evaluations of mangiferin-loaded PLGA scaffolds for alveolar bone repair treatment under the diabetic condition. AAPS PharmSciTech 2017; 18: 529-538.
[19] Fernandez-Sanchez L, Bravo-Osuna I, Lax P, Arranz-Romera A, Maneu V, Esteban-Perez S, Pinilla I, Puebla-Gonzalez MD, Herrero-Vanrell R and Cuenca N. Controlled delivery of tauroursodeoxycholic acid from biodegradable microspheres slows retinal degeneration and vision loss in P23H rats. PLoS One 2017; 12: e0177998.
[20] Ruan J, Wang X, Yu Z, Wang Z, Xie Q, Zhang DD, Huang YZ, Zhou HF, Bi XP, Xiao CW, Gu P and Fan XQ. Enhanced physiochemical and mechanical performance of chitosan-grafted graphene oxide for superior osteoinductivity. Adv Funct Mater 2016; 26: 1085-1097.
[21] Zhang W, Chang Q, Xu L, Li G, Yang G, Ding X, Wang X, Cui D and Jiang X. Graphene oxide-copper nanocomposite-coated porous CaP scaffold for vascularized bone regeneration via activation of Hif-1alpha. Adv Healthc Mater 2016; 5: 1299-1309.
[22] Karthikeyan R, Kanimozhi G, Prasad NR, Agilan B, Ganesan M, Mohana S and Srithar G. 7-Hydroxycoumarin prevents UVB-induced activation of NF-kappaB and subsequent overexpression of matrix metalloproteinases and inflammatory markers in human dermal fibroblast cells. J Photochem Photobiol B 2016; 161: 170-176.
[23] Hu J, Wang F, Sun R, Wang Z, Yu X, Wang L, Gao H, Zhao W, Yan S and Wang Y. Effect of combined therapy of human Wharton's jelly-derived mesenchymal stem cells from umbilical cord with sitagliptin in type 2 diabetic rats. Endocrine 2014; 45: 279-287.
[24] Stein J, Steven S, Bros M, Sudowe S, Hausding M, Oelze M, Munzel T, Grabbe S, Reske-Kunz A and Daiber A. Role of protein kinase C and Nox2-derived reactive oxygen species formation in the activation and maturation of dendritic cells by phorbol ester and lipopolysaccharide. Oxid Med Cell Longev 2017; 2017: 4157213.
[25] Jiang Y, Sang Y and Qiu Q. microRNA-383 mediates high glucose-induced oxidative stress and apoptosis in retinal pigment epithelial cells by repressing peroxiredoxin 3. Am J Transl Res 2017; 9: 2374-2383.
[26] Liu JT, Chen HY, Chen WC, Man KM and Chen YH. Red yeast rice protects circulating bone marrow-derived proangiogenic cells against high-glucose-induced senescence and oxidative stress: the role of heme oxygenase-1. Oxid Med Cell Longev 2017; 2017: 3831750.

[27] Exner M, Hermann M, Hofbauer R, Kapiotis S, Quehenberger P, Speiser W, Held I and Gmeiner BM. Genistein prevents the glucose autoxidation mediated atherogenic modification of low density lipoprotein. Free Radic Res 2001; 34: 101-112.
[28] Bonnefont-Rousselot D, Beaudeux JL, Therond P, Peynet J, Legrand A and Delattre J. [Diabetes mellitus, oxidative stress and advanced glycation endproducts]. Ann Pharm Fr 2004; 62: 147-157.
[29] Wolff SP and Dean RT. Glucose autoxidation and protein modification. The potential role of 'autoxidative glycosylation' in diabetes. Biochem J 1987; 245: 243-250.
[30] Liu Y, Yang H, Wen Y, Li B, Zhao Y, Xing J, Zhang M and Chen Y. Nrf2 inhibits periodontal ligament stem cell apoptosis under excessive oxidative stress. Int J Mol Sci 2017; 18.
[31] Ma XY, Feng YF, Ma ZS, Li X, Wang J, Wang L and Lei W. The promotion of osteointegration under diabetic conditions using chitosan/hydroxyapatite composite coating on porous titanium surfaces. Biomaterials 2014; 35: 7259-7270.
[32] Du L, Yang S, Li W, Li H, Feng S, Zeng R, Yu B, Xiao L, Nie HY and Tu M. Scaffold composed of porous vancomycin-loaded poly(lactide-co-glycolide) microspheres: a controlled-release drug delivery system with shape-memory effect. Mater Sci Eng C Mater Biol Appl 2017; 78: 1172-1178.
[33] Xiaoqin H, Zhang J, Tang X, Li M, Ma S, Liu C, Yue G, Zhang Y, Liu Y, Yu F, Yang Y, Jia G, Li Z, Mei X. An accelerated release method of risperidone loaded PLGA microspheres with good IVIVC. Curr Drug Deliv 2017; [Epub ahead of print].
[34] Huang J, Chen Z, Li Y, Li L and Zhang G. Rifapentine-linezolid-loaded PLGA microspheres for interventional therapy of cavitary pulmonary tuberculosis: preparation and in vitro characterization. Drug Des Devel Ther 2017; 11: 585-592.
[35] Hutmacher DW. Scaffolds in tissue engineering bone and cartilage. Biomaterials 2000; 21: 2529-2543.
[36] Hollister SJ. Porous scaffold design for tissue engineering. Nat Mater 2005; 4: 518-524.
[37] Yoo D. New paradigms in hierarchical porous scaffold design for tissue engineering. Mater Sci Eng C Mater Biol Appl 2013; 33: 1759-1772.